

# PROCEEDINGS OF SPIE

[SPIDigitalLibrary.org/conference-proceedings-of-spie](https://SPIDigitalLibrary.org/conference-proceedings-of-spie)

## Impact of mask topography and flare on process window of EUV lithography

Zhao, Rongbo, Dong, Lisong, Chen, Rui, Wei, Yayi

Rongbo Zhao, Lisong Dong, Rui Chen, Yayi Wei, "Impact of mask topography and flare on process window of EUV lithography," Proc. SPIE 11147, International Conference on Extreme Ultraviolet Lithography 2019, 111471V (26 September 2019); doi: 10.1117/12.2536871

**SPIE.**

Event: SPIE Photomask Technology + EUV Lithography, 2019, Monterey, California, United States

# Impact of mask topography and flare on process window of EUV lithography

Rongbo Zhao<sup>a,b</sup>, Lisong Dong<sup>a</sup>, Rui Chen<sup>a</sup>, Yayi Wei<sup>\*a,b</sup>

<sup>a</sup>Institute of Microelectronics, Chinese Academy of Sciences, Beijing 100029, China;

<sup>b</sup>University of Chinese Academy of Sciences, Beijing, 100049, China

## ABSTRACT

Mask three-dimensional effect (M3D) and flare are the critical issues for lithography in advanced technology nodes, especially for the extreme ultraviolet lithography (EUVL). The M3D effect leads to a shrinkage of critical dimension (CD) and the flare causes the unwanted background exposure. To evaluate impact of these two effects on EUVL performances, the process windows (PWs) of various test patterns under nominal condition are firstly simulated. And then an optimal source is selected by comparing PW values. At last, M3D is introduced by considering absorber thickness, and the flare is introduced by adding a constant distribution across the exposure field. All simulations are implemented by employing SLitho, a commercial software from Synopsys. The test patterns in simulations include line space, tip2tip and tip2line patterns, and the gaps of tip2tip and tip2line are 40, 45 and 50nm. The results of simulation show that mask topography will reduce the DOFs of test patterns, and constant flare has almost no effect on the DOFs of many test patterns.

**Keywords:** EUV, M3D, flare, simulation, process window

## 1. INTRODUCTION

For 5nm technology node and beyond, EUVL is regarded as the most promising lithography technology<sup>1</sup>. Differ from the deep ultraviolet lithography (DUVL), extreme ultraviolet lithography (EUVL) uses a very short wavelength. As the huge absorption of materials under this wavelength, the reflective mask and optics are employed in EUVL. The illuminator adopts oblique incidence (the chief ray angle at object is 6 degrees) and mask topography leads to the shadowing effect<sup>2-4</sup>. This effect can cause the shift of best focus (BF)<sup>5,6</sup>, horizontal and vertical bias (HVB) of lines<sup>3</sup> and the error of pattern placement<sup>7</sup>. The shadowing effect of mask is proportional to the thickness of absorber. Therefore, the absorber thickness needs to be optimized to reduce the shift of BF induced by M3D effect<sup>6</sup>. By comparing the process windows (PWs), the material of absorber is investigated to mitigate the M3D effect<sup>8</sup>. In addition, flare is more prominent in EUVL. It is caused by the surface roughness of the mirrors, and its amount is inversely proportional to the wavelength square<sup>9</sup>. The shorter wavelength will introduce larger amount of flare, and flare will cause unwanted background exposure<sup>10</sup>. In order to better analyze the effect of flare, four methods of ZRAM, MTF, Kirk and double exposure are presented by Sun et al<sup>11</sup>. A novel method of non-linear conversion for accurately predicting flare is proposed by Shiraishi in 2010<sup>9</sup>.

In this paper, the impacts of mask topography and flare on PWs of different test patterns are systematically investigated. Firstly, the optimal source map is predicted from the comparison of PWs for different mask patterns. Various illumination conditions are evaluated, including annular, dipole, quasar, conventional and so on. With optimal illumination, the PWs of test patterns with different settings of flare and mask topography are then calculated and compared. The settings of mask topography and flare are divided into four groups: no mask topography, no flare; no mask topography, with flare; with

---

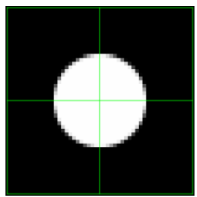
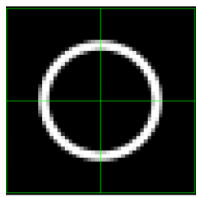
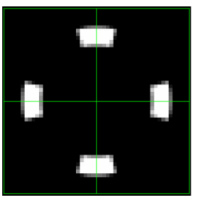
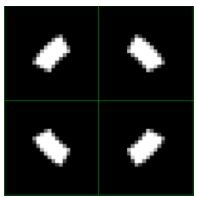
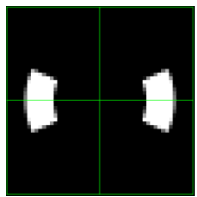
\* E-mail address: weiyayi@ime.ac.cn

mask topography, no flare; with mask topography, with flare. Finally, the influences of mask topography and flare on PWs of test patterns are summarized.

2. DETERMINATION OF OPTIMAL ILLUMINATION

In this simulation, we select three types of test patterns, including line space (L/S), tip2tip, tip2line. The critical dimension (CD) of test patterns is set as 16nm. To obtain the maximal PW, different source maps are employed in simulations. The source maps of annular, dipole, quasar, conventional sources are illustrated in Table 1.

Table 1. Diagrams of different source maps

Conventional	Annular	Quasar with rotation angle 0°	Quasar with rotation angle 45°	Dipole
				

To determine the optimal illumination, the PWs of test patterns under different source maps with different sigma are firstly calculated. Then the number of case when depth of focus (DOF) is greater than 80nm is counted at the corresponding sigma. After that, the optimal sigma is obtained and the corresponding PWs are compared for different illuminations. The rule of assessment is that the more the DOF goes larger than 80nm, the better, and the larger the minimal DOF of test patterns, the better at certain sigma. The optimal source map of illumination for test patterns is determined by comparing the PWs. In this paper, we only present the process of determining the optimal settings of annular and quasar illuminations.

The main simulation settings are listed as follows: the wavelength is 13.5nm, the numerical aperture (NA) of projector is 0.33, threshold is set to 0.1, EL is fixed at 5%, incident angle is 6 degrees, pupil reduction is 4 and absorber stack material is Ta<sub>6</sub>N<sub>4</sub>.

To obtain the PWs of test patterns, firstly, we set the illumination width to 0.1, 0.2, 0.3, and change the sigma to calculate DOFs, respectively. The DOFs of test patterns employing quasar illumination with width 0.1, 0.2 and 0.3 are gained when the angle is set to 30° as illustrated in Figure 1. In this figure, all test patterns have larger DOFs when the center radii are 0.75, 0.7 and 0.75, respectively. Then the DOFs are compared, and the optimal settings are determined that the quasar width is 0.2, and the center radius is 0.7. Based on the optimal quasar width and center radius determined above, the PWs of test patterns are calculated in different angles as illustrated in Figure 2. In the figure, all test patterns can reach larger DOFs when the angle is about 30°, and it is considered as the optimal angle.

Employing the similar method, firstly, the width of annular illumination is fixed at 0.1, 0.2, 0.3, and the optimal center radii of these three situations are all determined as 0.6 as shown in Figure 3. By comparison, the optimal settings of annular illumination are determined to be that the width is 0.1, and the center radius is 0.6. To obtain the optimal source map of illumination, the maximal DOFs of test patterns for annular and quasar illuminations are compared. The minimal DOF of test patterns for quasar illumination with optimal settings is 93.17nm which is greater than the 90.46nm for annular illumination. Therefore, quasar is regarded as the optimal illumination of all test patterns, and the corresponding settings

are that the inner radius is 0.6, the outer radius is 0.8, and the angle and rotation angle are  $30^\circ$  and  $45^\circ$ , respectively as illustrated in Figure 4.

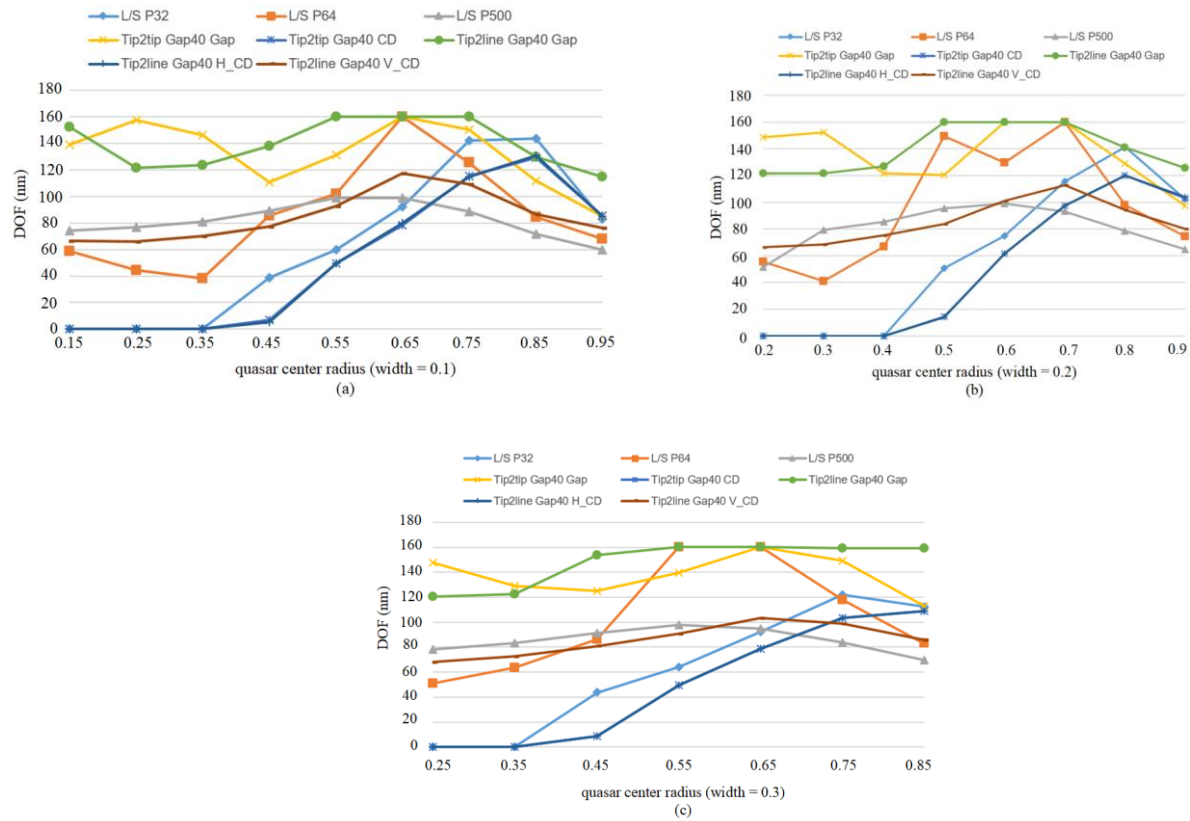


Figure 1. DOFs of quasar illumination with (a) width 0.1 (b) width 0.2 (c) width 0.3.

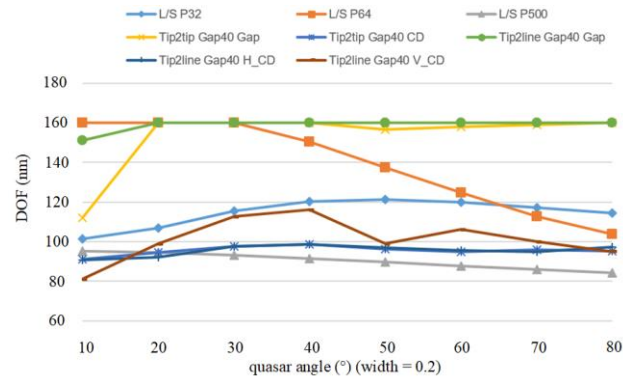


Figure 2. DOFs of quasar illumination with width 0.2 and different angles.

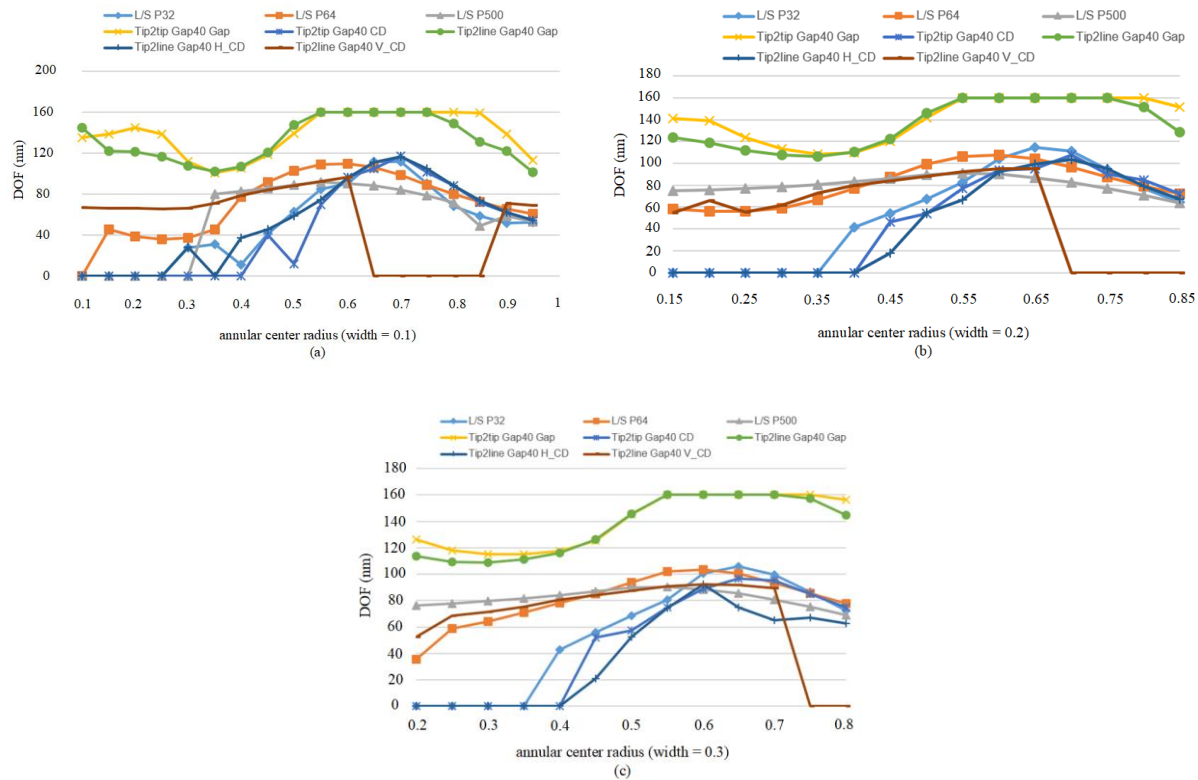


Figure 3. DOFs of annular illumination with (a) width 0.1 (b) width 0.2 (c) width 0.3.

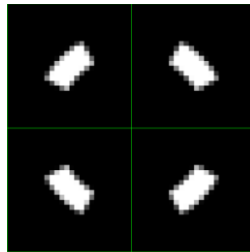


Figure 4. Optimal quasar source map.

### 3. IMPACT OF MASK TOPOGRAPHY AND FLARE ON PROCESS WINDOW

To investigate the impact of mask topography and flare on PWs, we select three types of test patterns including L/S with different pitches, tip2tip and tip2line with gaps 40, 45 and 50 nm. The settings of mask topography and flare are divided into four categories: no mask topography, no flare; no mask topography, with flare; with mask topography, no flare; with mask topography, with flare. And the PWs of all 21 test patterns are calculated and compared in these four situations, respectively.

#### 3.1 Determination of optimal mask topography thickness

To better evaluate the effect of mask topography on PWs, we change the thickness of mask topography to calculate the DOFs of test patterns. In this simulation, flare is set to 4% according to the NXE extension roadmap<sup>6</sup>. The DOFs of all test patterns with different thickness are presented in Figure 5. As illustrated in this figure, all test patterns can reach larger

DOFs when the thickness of topography is about 15 nm, i.e., wafer scale thickness. If the thickness is less than 15 nm, it exhibits poor imaging performance in EUVL. Moreover, it can cause prominent shadowing effect when the thickness is greater than 15 nm. Therefore, we conclude that 15 nm is considered as the optimal thickness of mask topography.

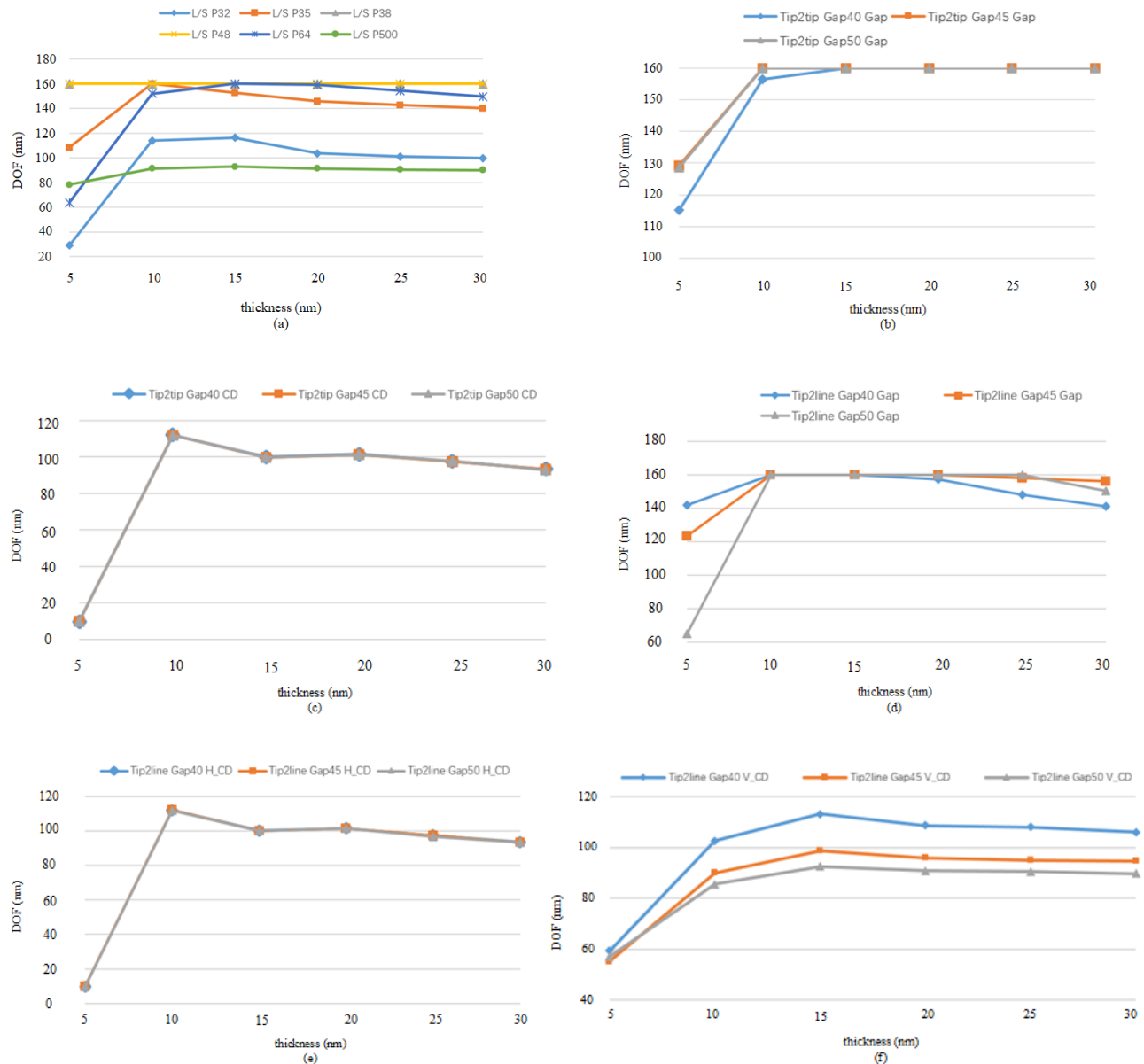


Figure 5. DOFs through thickness of (a) L/S (b) tip2tip gap (c) tip2tip CD (d) tip2line gap (e) tip2line horizontal CD (f) tip2line vertical CD.

### 3.2 Effect of mask topography and flare on DOFs

Adopting the optimal thickness determined above, the DOFs of L/S with variable pitches are presented in Figure 6. As shown in this figure, mask topography can reduce the DOFs of L/S except for a few special pitches, such as pitches 32, 34, 36 nm and so on. With flare, it presents smaller DOFs for L/S patterns. For patterns of tip2tip with gaps 40, 45 and 50 nm,

the DOFs of gap and CD are reduced with flare. However, mask topography enlarges the DOFs compared with thin mask as illustrated in Figure 7. Employing the similar method, the DOFs of tip2line with gaps 40, 45 and 50 nm are calculated as shown in Figure 8. From the figure, with flare, the DOFs become smaller, and mask topography reduces the DOFs except for the test patterns of tip2line horizontal CD with gaps 40, 45 and 50 nm.

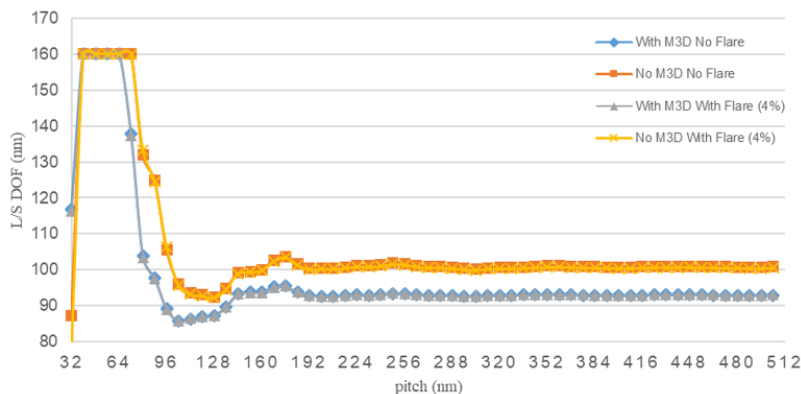


Figure 6. L/S DOFs through pitch with different settings of mask topography and flare.

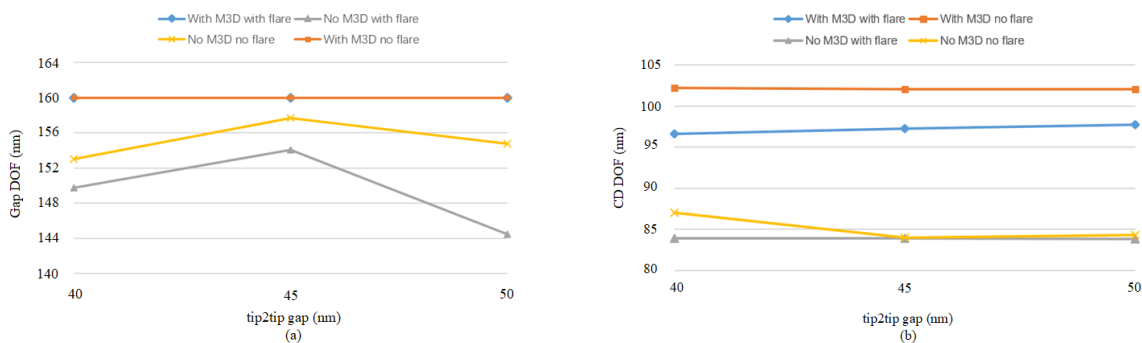
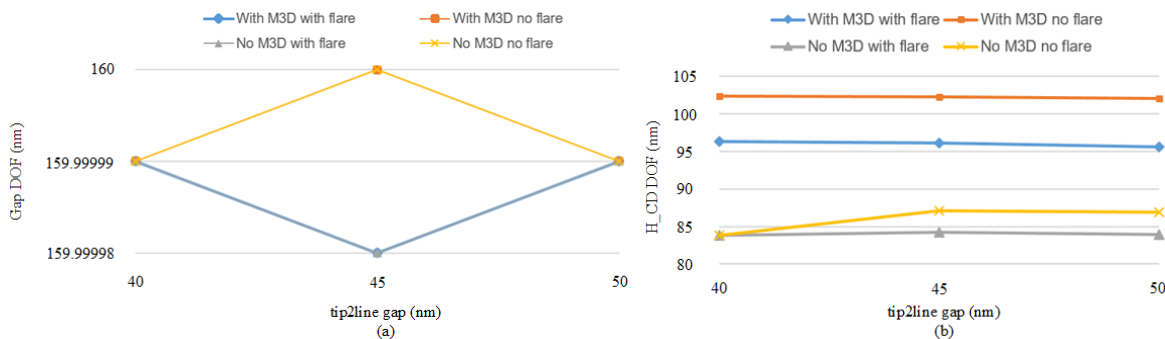


Figure 7. DOFs with different settings of mask and flare of (a) tip2tip gap (b) tip2tip CD.



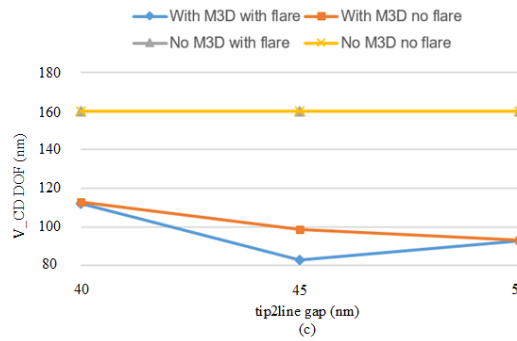


Figure 8. DOFs with different settings of mask and flare of (a) tip2line gap (b) tip2line horizontal CD (c) tip2line vertical CD.

To investigate the effect of the amount of flare on PW in EUVL, we change the flare of TIS short range in Slitho simulator to calculate the DOFs of test patterns with the optimal thickness of mask topography. The range is set from 0 to 10%, and the DOFs of test patterns are presented in the following figures.

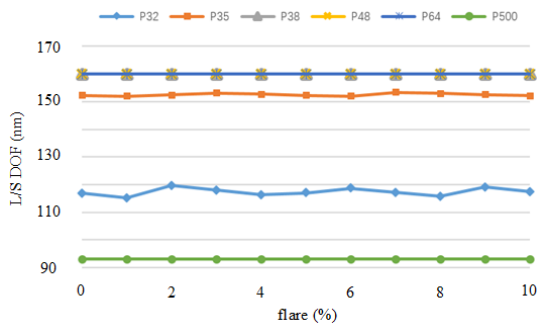


Figure 9. L/S DOFs with variable flare.

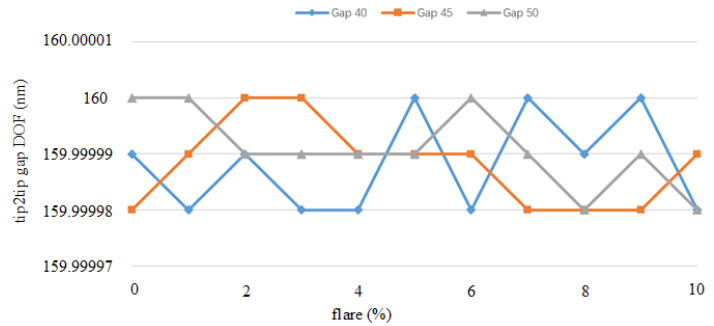


Figure 10. Tip2tip gap DOFs with variable flare.

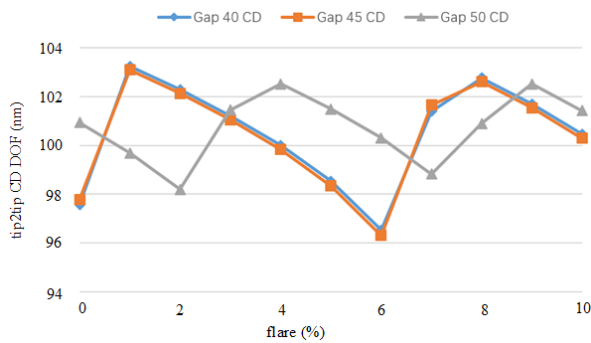


Figure 11. Tip2tip CD DOFs with variable flare.

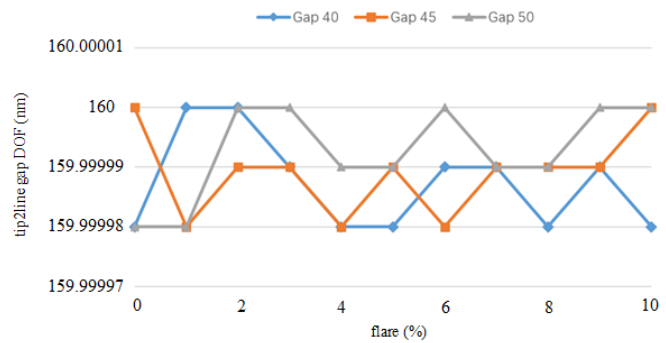


Figure 12. Tip2line gap DOFs with variable flare.



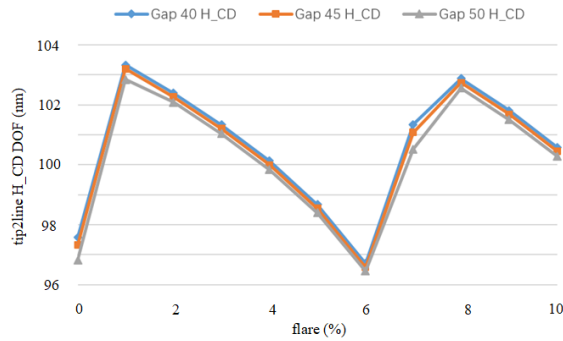


Figure 13. Tip2line horizontal CD DOFs with variable flare.

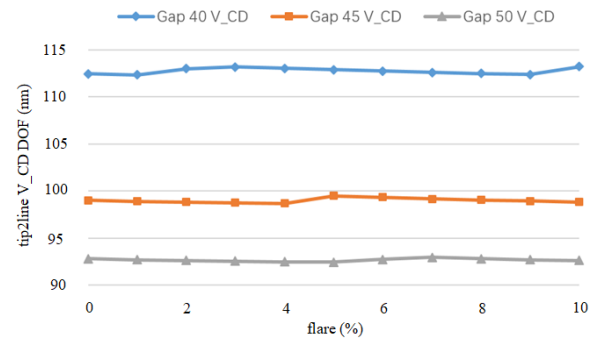


Figure 14. Tip2line vertical CD DOFs with variable flare.

Overall, the DOFs of all test pattern vary insignificantly with increasing flare compared with M3D effect. For L/S test patterns, the DOFs with pitches 32 and 500 nm have smaller value, and the DOF is minimum when the pitch is 500 nm as shown in Figure 9. The variation of DOFs for tip2tip gap test patterns is rather small and they have almost reached the maximum as illustrated in Figures 10. The trend is consistent for tip2tip CD with gaps 40 and 45 nm, that is, it increases first and then decreases when the flare is from 0 to 10%. And these two patterns have the minimal DOFs when the flare is set to 6%. However, it presents opposite trend for the tip2tip CD with gap 50 nm as shown in Figure 11. Similar to the patterns of tip2tip gap, the effect of flare on DOFs of tip2line gap patterns is not prominent, and they behave perfect imaging performance as illustrated in Figure 12. In Figure 13, it presents identical trend of variation for DOFs of tip2line horizontal CD, and the PWs present poor result when the flare is fixed at 6%. For the test patterns of tip2line vertical CD, the variation of DOFs with different flare is not pronounced, and the DOFs decrease while the gap increases as shown in Figure 14.

#### 4. CONCLUSION

By employing the different mask patterns of L/S, tip2tip and tip2line, and comparing the PWs under different illumination conditions, the optimal source map and parameters are determined as quasar with rotation angle  $45^\circ$ . Then the settings of mask topography and flare are divided into four groups to evaluate their impact on lithography performance, the groups are featured with: no mask topography, no flare; no mask topography, with flare; with mask topography, no flare; with mask topography, with flare. The thickness of mask absorber in the latter two groups is determined by setting this parameter as variable and comparing the DOFs of test patterns under different mask topography conditions. With optimal illumination, the PWs of test patterns with different settings of flare and mask topography are calculated. By comparing the lithography imaging performance, it can be inferred that the mask topography will reduce the DOFs of line space patterns, and the constant flare with 4% has almost no impact on the DOFs of test patterns. In addition, the impacts of the amount of flare on PW are also investigated. From the simulation results, the conclusion of constant flare had very little influence on DOFs of selected test patterns. In our future work, the impact of non-constant flare map across exposure field will be evaluated.

#### ACKNOWLEDGEMENT

This work is supported by the National Science and Technology Major Project of China (Grant No. 2017ZX02315001-003), and the National Natural Science Foundation of China under No. 61804174. We also thank EUV lithography

## REFERENCES

- [1] Kamo, T.; Aoyama, H.; Tanaka, T.; Suga, O., "Effects of mask absorber thickness on printability in EUV lithography with high resolution resist," Proc. SPIE 7028, Photomask and Next-Generation Lithography Mask Technology XV, 70281R (2008).
- [2] Kang, H.; Hansen, S.; Schoot, J. v.; Schenau, K. v. I., "EUV simulation extension study for mask shadowing effect and its correction," Proc. SPIE 6921, Emerging Lithographic Technologies XII, 692131 (2008).
- [3] Ruoff, J., "Impact of mask topography and multilayer stack on high NA imaging of EUV masks," Proc. SPIE 7823, Photomask Technology, 78231N (2010).
- [4] Song, H.; Zavyalova, L.; Su, I.; Shiely, J.; Schmoeller, T., "Shadowing effect modeling and compensation for EUV lithography," Proc. SPIE 7969, Extreme Ultraviolet (EUV) Lithography II, 79691O (2011).
- [5] Liu, P., "Accurate prediction of 3D mask topography induced best focus variation in full-chip photolithography applications," Proc. SPIE 8166, Photomask Technology, 816640 (2011).
- [6] Davydova, N.; Setten, E. v.; Kruif, R. d.; Connolly, B.; Fukugami, N.; Kodera, Y.; Morimoto, H.; Sakata, Y.; Kotani, J.; Kondo, S.; Imoto, T.; Rolff, H.; Ullrich, A.; Lammers, A.; Schiffelers, G.; Dijk, J. v., "Achievements and challenges of EUV mask imaging," Proc. SPIE 9256, Photomask and Next-Generation Lithography Mask Technology XXI, 925602 (2014).
- [7] Davydova, N.; Setten, E. v.; Han, S.-I.; Kerkhof, M. v. d.; Kruif, R. d.; Oorschot, D.; Zimmerman, J.; Lammers, A.; Connolly, B.; Driessen, F.; Oosten, A. v.; Dusa, M.; Dommelen, Y. v.; Harned, N.; Jiang, J.; Liu, W.; Kang, H.; Liu, H.-y., "Mask aspects of EUVL imaging at 27nm node and below," Proc. SPIE 8166, Photomask Technology, 816624 (2011).
- [8] Philipsen, V.; Luong, K. V.; Souriau, L.; Hendrickx, E.; Erdmann, A.; Xu, D.; Evanschitzky, P.; Kruijs, R. W. E. v. d.; Edrisi, A.; Scholze, F.; Laubis, C.; Irmscher, M.; Naasz, S.; Reuter, C., "Reducing EUV mask 3D effects by alternative metal absorbers," Proc. SPIE 10143, Extreme Ultraviolet (EUV) Lithography VIII, 1014310 (2017).
- [9] Shiraishi, M.; Oshino, T.; Murakami, K.; Chiba, H., "Flare modeling and calculation on EUV optics," Proc. SPIE 7636, Extreme Ultraviolet (EUV) Lithography, 763629 (2010).
- [10] V, J. W.; Belledent, J.; Trouiller, Y.; Maurer, W.; Granik, Y.; Sahouria, E.; Touban, O., "Full-chip model-based correction of flare-induced linewidth variation," Proc. SPIE 5567, 24<sup>th</sup> Annual BACUS Symposium on Photomask Technology (2004).
- [11] Sun, L.; Il, O. R. W.; Verduijn, E. A.; Singh, M.; Wang, W.; Kim, R.-H.; Mangat, P. J.; Koh, H. P.; Levinson, H. J., "Review of resist-based flare measurement methods for extreme ultraviolet lithography," Journal of Micro/Nanolithography, MEMS, and MOEMS, 12(4), 042001 (2013).